Femtochemistry at high pressures. The dynamics of an elementary reaction in the gas–liquid transition region

Ch. Lienau [1], J.C. Williamson [2] and A.H. Zewail

Arthur Amos Noyes Laboratory of Chemical Physics [3], California Institute of Technology, Pasadena, CA 91125, USA

Received 2 August 1993

An extension of femtochemistry to the gas–liquid transition region is reported for an elementary reaction, the dissociation and recombination of iodine in supercritical argon reaching a density of 30.5 mol ℓ^{-1}. Three phenomena are systematically studied in the range 0 to 2000 bar of argon: the change of the coherent nuclear motion with solvent density, the rate of predissociation, and the caging by the solvent. The approach offers a unique way for examining the dynamics in real time from the gas to the liquid density limit.

1. Introduction

In this Letter, studies of the real-time dynamics of an elementary chemical reaction in the gas to liquid density transition are reported. Using femtosecond transition-state spectroscopy (FTS), we probed the dissociation and recombination of iodine in supercritical argon over a wide range of pressures. Variation of the argon pressure smoothly changes the behavior of the solvent, from an essentially ideal gas at low pressures to a liquid-like fluid at pressures of several thousand atmospheres. In this way, the collision time between iodine molecules and argon atoms is gradually brought to the time scale of the nuclear motion of the solute iodine. With femtosecond resolution, this approach offers an opportunity to study in real time the change in the dynamics of the coherent wave packet (nuclear) motion, the electronic predissociation, and the caging by the solvent, from the collision-free to the liquid phase limit.

We have chosen iodine as a prototype system for a number of reasons. The recombination of the two photodissociated iodine atoms in solution has been the focus of many studies over the past 60 years [1–3]. Furthermore, there is a wealth of information available on the dynamics of this system in the two limiting phases of our study: the collisionless gas phase and the liquid phase. Studies of iodine dynamics in the cluster phase have also been reported, as discussed below.

For argon-free iodine, the wave packet dynamics in the bound $B(^3\Pi_{0^+u})$ state and on the repulsive $^1\Pi_u$ and $A(^3\Pi_{1u})$ states have been studied on the femtosecond time scale [4]. On the B state the coherent nuclear motion persists and shows the period of the oscillation between the turning points of the potential; from these studies one obtains the potential of the motion [5]. Time-resolved studies have also been reported for rare gases compressed to 100 bar [6]. Molecular dynamics simulations by Wilson's group [7] gave good agreement with the experimental results. These early studies at 100 bar showed the effect of the argon collisions on the vibrational coherence of the wave packet, the collision-induced B-state predissociation on a time scale of several picoseconds, as well as "caging" of I_2 molecules excited above the B-state dissociation threshold. Earlier experiments by the groups of Troe [8] and van den Bergh [9] on the photolysis quantum yield of iodine

[1] Deutsche Forschungsgemeinschaft Postdoctoral Fellow.
[2] National Science Foundation Predoctoral Fellow.
[3] Contribution No. 8831.

0009-2614/93/$ 06.00 © 1993 Elsevier Science Publishers B.V. All rights reserved.

and bromine in a number of solvents indicated the onset of the "photolytic cage effect" at surprisingly low gas pressures. This effect was attributed to the presence of a large amount of van der Waals clusters at the relevant densities [10]. In clusters of argon, it has recently been shown that the caging dynamics is determined by the initial time scale of bond breakage relative to solvent rearrangement [11].

In liquids, studies of picosecond dynamics began with Eisenthal's early experiments on iodine recombination [12]. Our understanding of vibrational relaxation following caging has improved considerably, both theoretically [13] and experimentally [14–17], and the review by Harris [18] describes this progress. From transient absorption experiments, Harris et al. [16,18] have shown that the B-state excitation leads to the formation of highly vibrationally excited X- or A-state products in less than two picoseconds. The experiments elucidated the vibrational relaxation dynamics on the ground state as well as on the A/A′ states. The nature of the electronic states involved in the electronic predissociation in solution, however, is not fully understood.

Scherer et al. [19] showed that the dephasing time is approximately 0.3 ps on the B state, consistent with the resonance Raman studies by Sension and Strauss [20] (see also ref. [6]). The detected signal in ref. [19] is a superposition of the ground and excited state wave packet motion. The analysis of these results indicates that the dephasing is caused by electronic predissociation. (The experiments have not yet probed the caging dynamics.) The dynamics of the wave packet dephasing in the iodine system is a much different process than the optical dephasing in large systems, probed directly in real time by the groups of Shank [21], Wiersma [22] and others. In clusters of argon [11], when the dissociation time is on the femtosecond time scale, a coherent caging was observed on the subpicosecond time scale, but on the B state the picture is very different due to electronic predissociation, as discussed below.

Here, we address the issues of predissociation, caging, and nuclear motions at different solvent densities using two-color real-time probing of I_2 dynamics in highly compressed (supercritical) argon. Laser-induced fluorescence detection is used in order to monitor the wave packet motion *only* on the state of interest (B), as we did in the isolated system [4]. The argon density at 2000 bar is 30.5 mol ℓ^{-1}, which corresponds to approximately 18 argon atoms per nm^3; this density is 750 times larger than the density at 1 bar, and is close to the density of liquid argon at the triple point (35.4 mol ℓ^{-1}) [23]. In our experiments we use a 60 fs laser pulse, centered at 620 nm, to excite ground state I_2 molecules. Nearly 62% of the excited molecules reach vibrational levels $v'=6$–11 of the bound B state [4,5], while 34% of the molecules are placed on the weakly bound A state and the rest on the dissociative $^1\Pi$ state [24]. The dynamics of the prepared wave packet are probed by a second 310 nm pulse, which excites the B-state molecules to either the E $^3\Pi(0_g^+)$ or f(0_g^+) ion-pair states [25]. The optical signal is obtained by collecting the fluorescence from the ion-pair state(s). If argon is present, a rapid electronic quenching [26] from the E or f to the D′ state is induced so that the detected fluorescence comes from the strong D′→A′ transition [27].

2. Experimental

The 60 fs laser pulses were generated from a colliding-pulse mode-locked ring dye laser (CPM) and amplified in a four-stage, Nd:YAG-pumped dye amplifier (PDA). The design of a similar CPM/amplifier system has been discussed in greater detail elsewhere [28]. The amplified pulses were temporally recompressed in a double-pass, two-prism arrangement before being separated into pump and probe lasers by a 50/50 beam splitter (fig. 1). Together, the pump and probe lasers formed two arms of a Michelson interferometer. The probe laser was focused into a KD*P crystal to generate the 310 nm pulse, and the fundamental was removed with a UG 11 filter. The pump and probe lasers were recombined with a dichroic beam splitter and then focused slightly beyond the center of the high-pressure cell to avoid continuum generation. Laser-induced fluorescence was collected perpendicular to the laser propagation direction, collimated into a monochromator, and detected on a PMT. The relative timing between the two pulses was varied with a high-precision, computer-controlled actuator located in the path of the pump laser. The pump arm also contained two polarizers and a half-wave plate to allow variation in

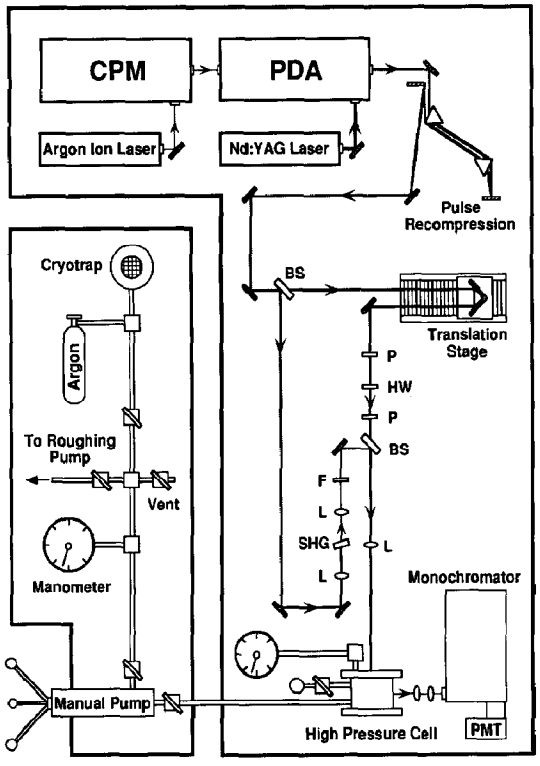

Fig. 1. Overall schematic of the apparatus used in the high-pressure studies. CPM: colliding-pulse mode-locked dye laser; PDA: four-stage pulsed dye amplifier; BS: beamsplitter; L: lens; SHG: second harmonic generation crystal; F: filter; P: polarizer; HW: half-wave plate; PMT: photomultiplier tube.

the angle between the polarizations of the two lasers, and this angle was kept constant at 54.7° (the "magic" angle) to remove rotational anisotropy effects from the transients. Studies of the anisotropy at high pressures will be discussed elsewhere.

The high-pressure cell was constructed from stainless steel and designed to withstand pressures of up to 4000 bar. Details of the design and the precision measurements will be given in a full account of this work. Four windows, 6 mm in diameter, were centered in each of the four walls, and the cell had a total volume of 0.2 cm^3. The input window was 4.0 mm thick quartz, while the output and fluorescence-collection windows were 2.8 mm thick sapphire. Pressure in the cell was monitored with a precision strain gauge pressure transducer. Care was taken when introducing iodine into the cell. The cell was then filled with argon gas, which was compressed to the desired pressure in an iterative process. To reach pressures above 1200 bar, the argon gas was precompressed to 400 bar by liquifying the argon in a pressure-resistant cryotrap. The high-pressure cell showed no decrease in argon pressure during the course of an experiment.

Fluorescence signal from the PMT was averaged in a boxcar integrator and recorded as a function of actuator position in a computer. The transients were fitted to the single exponential decay and the biexponential rise using standard programs which take into account the 60 fs pulse widths. At each pressure, a set of transients obtained over different time intervals (4, 20, and 200 ps) were globally fitted using identical parameters.

We observed a pressure-induced shift in the D′→A′ fluorescence spectrum. The maximum shifted from 340 nm at 0 bar to 374 nm at 2000 bar. This shift of the ion-pair state with solvation is consistent with similar observations in the liquid phase [18] and in rare gas clusters [11,29]. The change in the refractive index with pressure was also observed.

3. Results and discussion

3.1. Wave packet dynamics

Excitation of iodine molecules at room temperature with a 60 fs, 620 nm pump pulse leads to the formation of a wave packet at the inner turning point of the B-state potential. This wave packet consists of a coherent superposition of vibrational eigenstates $v'=6$–11 centered around $v'=8$ [5]. For isolated molecules, this wave packet freely propagates on the B-state potential surface, and its oscillatory motion can be probed in real time with a second femtosecond laser pulse [4]. The anharmonicity of the excited potential leads to an interference pattern with a recurrence period of about 9 ps, as observed at zero (argon) pressure in figs. 2 and 3.

The effect of iodine–argon collisions on the B-state wave packet coherence is shown in fig. 2. Vibrational coherence persists for more than 1.5 ps (≈five vibrational periods) at pressures as high as 800 bar, although the modulation depth decreases with pressure. (This decrease is partly due to dispersive temporal broadening of the laser pulses at higher pres-

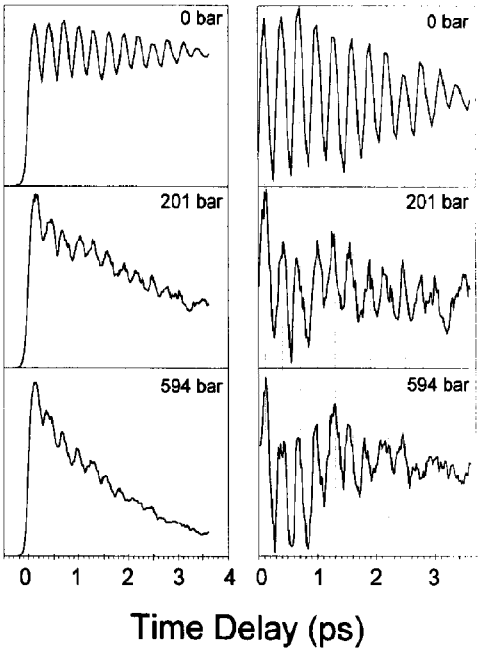

Fig. 2. Femtosecond transients of iodine in compressed supercritical argon at 295 K. Left: experimentally observed transients at argon pressures of 0, 201, and 594 bar using LIF detection at the "magic angle" (54.7°) between the pump and probe pulses. Fluorescence detection wavelength: 340 nm – 0 bar, 351 nm – 201 bar, and 360 nm – 594 bar. Right: the oscillatory component of the transients (wave packet motion) obtained by subtracting the underlying single exponential decay due to electronic predissociation. To accentuate the pressure-induced decrease in the vibrational frequency, we overlaid gridlines spaced at multiples of the mean oscillation period at 0 bar. Note that the decay of the envelope of the oscillation was not evaluated, as this requires careful Fourier analysis of the transient (see text), and will be discussed later.

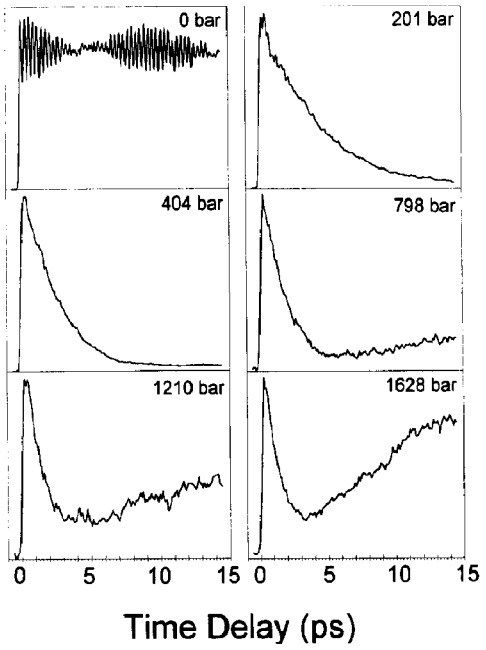

Fig. 3. Femtosecond transients (up to 15 ps) observed for excitation of the iodine in compressed supercritical argon at 295 K and various pressures. Fluorescence detection wavelength: 340 nm – 0 bar; 351 nm – 201 bar; 360 nm – 404 bar; 364 nm – 798 bar; 367 nm – 1210 bar; 370 nm – 1628 bar. Note the increase in the decay rate with increase in the pressure and the rise due to caging. Except for the 0 bar data, the stepsize used in these transients was too large to resolve the wave packet motion shown in fig. 2.

sures.) The persistence of the wave packet is somewhat surprising, since about four iodine bath-gas collisions occur per picosecond at 800 bar, evidently more than six collisions are required to destroy the vibrational coherence of the wave packet (see below).

Loss of vibrational coherence occurs on approximately the same time scale as the exponential decay of the transient. The exponential decay is due to collision-induced electronic predissociation of the B state, as will be discussed in section 3.2. Both the elastic and inelastic collisions should contribute to the total rate of dephasing [6]. Apparently, the elastic solute–solvent collisions have relatively less or comparable impact than energy-changing collisions on iodine. The dephasing due to the anharmonicity of the potential in the isolated I_2 is on the picosecond time scale. Since the packet has a discrete structure of vibrational levels, this dephasing is followed by a rephasing, also on the picosecond time scale. With argon, the "elastic" collisions will induce phase shifts that must be averaged over all solvent configurations. Considering the energy spread and the period, we estimate a dephasing time [6] on the order of 1 ps. These results will be quantified when the oscillatory motions are analyzed for all densities and in different solvents and the nature of the force field [30] is considered rigorously. Comparisons will be made to molecular dynamics simulations.

To address how the iodine oscillation period is affected by the presence of the argon gas, the underlying predissociation decay was subtracted and the fast Fourier transform was calculated. Due to the

small number of oscillations in the transient, the frequency resolution in the Fourier spectrum was low, and we were unable to resolve the frequencies of the different vibrational eigenstates (other methods [5] will be tested in the future). However, the maximum in the Fourier spectrum made a significant shift to higher frequencies with increasing pressure – from 111 cm^{-1} at 0 bar argon to about 118 cm^{-1} at 800 bar. The oscillation frequencies were also measured directly without Fourier transformation. If the B-state potential were unaffected by the solvent, this shift would imply that vibrational eigenstates with higher frequencies, and lower quantum numbers, were probed. These states would only be populated by vibrational relaxation, but it is unlikely that vibrational coherence would be preserved during these inelastic collisions.

Solvent-induced interactions generally cause a shift in the relative energy of potential energy surfaces, and a change in the equilibrium position and the frequency of vibrations. Such changes have been treated theoretically in a number of cases by the groups of Herschbach [31], Ben-Amotz [32], and others. In our case, the wave packet executes a large-amplitude motion and the sensitivity to solvent interactions at larger distances far from equilibrium must be taken into account. The shift of the wave packet oscillation frequency starts at lower pressures (from 0 to 200 bar) and this behavior may reflect large amplitudes of motion which we shall treat theoretically elsewhere. The shift increases with pressure and this behavior is consistent with solute bond contraction due to a repulsive force.

3.2. The predissociation dynamics

Decay of molecular iodine excited to the B state can be attributed to three competing processes (for a review, see ref. [33]): radiative decay with a lifetime τ_0, nonradiative decay due to predissociation induced via iodine–iodine collisions (characterized by the self-quenching rate $1/\tau_s$), and predissociation induced via iodine–argon collisions, characterized by a quenching rate $1/\tau_q$. For the experiments reported here, the argon–iodine collision-induced quenching rate is orders of magnitude faster than $1/\tau_s$ and $1/\tau_0$, and therefore dominates the B-state decay process.

According to the simple Stern–Volmer model, the collisional quenching rate is proportional to the bath-gas pressure and is given by

$$\frac{1}{\tau} = \sigma\left(\frac{8\pi}{\mu kT}\right)^{1/2} P. \qquad (1)$$

In this equation, σ denotes the quenching cross section, μ is the reduced mass of the collision partners, k is Boltzmann's constant, T is the temperature, and P is the pressure. The repulsive state populated by predissociation has not been conclusively identified, but it is likely to be either the a $(^3\Pi_{1g})$ or the a' $(^3\Sigma_g^-(0^+))$ state (see the recent discussion by Scherer et al. [19]). Both states cross the B state at low energies; $a1_g$ crosses near the outer turning point of $v'=1$ and $a'0_g^+$ crosses near $v'=5$.

The transients for molecular iodine at argon pressures between 0 and 2000 bar show that the B-state decay time decreases drastically with increasing pressure (fig. 3). The one ps decay rate at 2000 bar indicates that the predissociation rate at this limit of density is less than two picoseconds, suggested as an upper limit for liquid solvents [18]. It is also interesting to note that this measured time approaches the 0.3 ps predissociation time obtained by resonance Raman [20] and by pump–probe studies in methylcyclohexane [19]. For studies in carbon tetrachloride and comparison with 100 bar argon, see ref. [6].

Fig. 4c shows that at high pressures the experimentally determined predissociation rate deviates significantly from the Stern–Volmer model. This is not surprising since the density, and therefore also the collision frequency, is not proportional to pressure above 400 bar. Actually if the Stern–Volmer equation is rewritten to include the density, instead of the pressure, there is excellent agreement with experiment when a quenching cross section of 3.65 $Å^2$ is used (see fig. 4c); Capelle and Broida measured a quenching cross section of 5.62 $Å^2$ at an excitation wavelength of 623.4 nm for an argon pressure of 4×10^{-5} bar [35]. This consideration of change in density describes the collision-induced predissociation rate over a pressure range of almost eight orders of magnitude.

The above results on the change of the predissociation rates over the entire range of densities bring into focus another point regarding the dynamics of

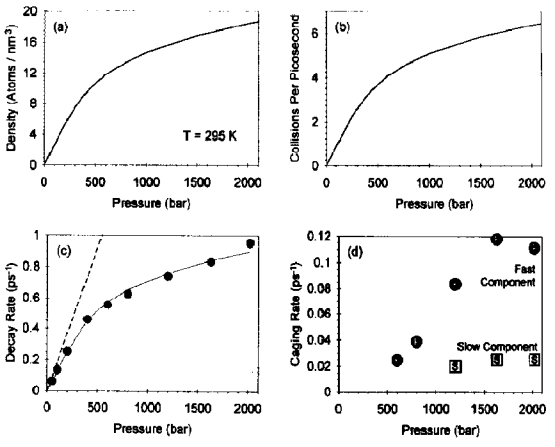

Fig. 4. (a) Argon density as a function of pressure measured at 295 K [23]. (b) Estimated frequency of iodine–argon collisons as a function of pressure (see e.g. ref. [34] and text), assuming a Lennard-Jones (6–12) interaction potential ($\epsilon = 209.7$ cm^{-1}, $\sigma = 3.59$ Å [11]). (c) Rate for collision-induced predissociation of iodine in argon at an excitation wavelength of 620 nm as a function of argon pressure. The dashed line shows the extrapolation of the Stern–Volmer equation (eq. (1)) using the Capelle–Broida low-pressure quenching cross section of 5.62 Å^2 [35]. The solid line is the predicted change of rate with pressure assuming that the collision frequency is proportional to density (see text). (d) The change of the inverse rise time with pressure. The rise is found to be single-exponential at argon pressures at 800 bar and below and biexponential at 1200 bar and above.

the collision. The rate of predissociation is a product of the frequency of collisions and the predissociation probability. From the experimentally determined rates and the change of density with pressure we obtain a pressure-independent probability of ≈ 0.1. The implication from this behavior is that the collision frequency is proportional to the density and that binary collisions are the key in the dynamics. However, to test this finding more carefully, the radial distribution function must be evaluated at different densities. Molecular dynamics simulations should be helpful to our understanding of this issue, particularly since the time scale of the dynamics is reaching the average time between collisions. The extent to which van der Waals complexes can be formed on this time scale is important to the description of the dephasing and caging.

3.3. The caging dynamics

In compressed gases, geminate recombination in the photodissociation of halogens has been experimentally verified via photolysis quantum yield measurements [8]. In the particular case of iodine in argon, early experiments by Luther and Troe indicated that geminate recombination was absent at pressures below 1000 bar [36]. Our real-time experimental transients, however, show that above 400 bar the fast decay of predissociation signal is followed by a slow rise, whose relative amplitude increases strongly with pressure (fig. 3). This rise reflects the cage effect, described by the geminate recombination of iodine atoms and the subsequent vibrational relaxation of the nascent iodine molecules. A 1 ns transient taken at 1600 bar (not shown) revealed that the signal intensity beyond 200 ps remains constant. A lower limit of at least 5 ns can thus be obtained for the lifetime of the observed electronic state.

The risetimes we measured in compressed argon range from 40 ps at 600 bar to less than 10 ps at 2000 bar. The rise appears to be biexponential at pressures above 1200 bar. As in similar studies in liquid xenon [16], the fast risetime is assigned to vibrational relaxation within the A/A′ states and the slow risetime to the A→A′ electronic curve-crossing dynamics. The rise indicates the recombination of the iodine atoms, but in order to separate contributions from the X and the A/A′ states, we plan further experiments with tunable probe pulses, as we did in argon clusters [11].

From fig. 4d, we note that the onset of caging occurs at pressures where the density begins to deviate strongly from that of an ideal gas. This reflects the threshold for formation of solvent cages. As the argon pressure increases, the solvent cages become more rigid and the probability for geminate recombination is larger. In the work on clusters [11] the rigidity of the solvent cage facilitated prompt caging, if the bond-breakage time is short compared to solvent rearrangement. Here, as the density increases we note an increase in the fast rise component. It will be interesting to follow such transitional changes with molecular dynamics simulations and compare with the results of the cluster work.

4. Conclusions

In this contribution the dissociation and recombination dynamics of iodine in supercritical argon is studied on the femtosecond time scale over a range covering the gas phase to the liquid state density. The wave packet motion on the iodine B-state surface maintains its coherence for several picoseconds at pressures as high as 800 bar. Furthermore, the collision-induced B-state predissociation rate increases with density and reaches 1 ps at the highest density (30.5 mol ℓ^{-1}) at 2000 bar. The reaction probability per collision, however, remains constant, reflecting the nature of the binary collisions and the radial distribution function. The onset of direct geminate recombination of the dissociating iodine atoms takes place at pressures above 400 bar, and the probability for "caging" increases with pressure. The study of this and other chemical reactions under these "controlled" density conditions presents a unique opportunity to learn about solute–solvent interactions. We are currently involved in related experimental and theoretical studies of these interactions in the gas–liquid interface region on the femtosecond time scale.

Acknowledgement

This work was supported by the National Science Foundation. We would like to thank Dr. Dirk Schwarzer of Professor J. Troe's group for helpful discussions and advice. We are grateful to Dr. Marcos Dantus for his valuable help in setting up the laser system in the initial stage of this work. ChL gratefully acknowledges a postdoctoral fellowship by the Deutsche Forschungsgemeinschaft, and JCW acknowledges the National Science Foundation for a Graduate Fellowship.

References

[1] J. Franck and E. Rabinowitch, Trans. Faraday Soc. 30 (1934) 120.

[2] L. Meadows and R.M. Noyes, J. Am. Chem. Soc. 82 (1960) 1872.

[3] G. Porter and J.A. Smith, Proc. Royal Soc. A 261 (1961) 28;
D.L. Bunker and N. Davidson, J. Am. Chem. Soc. 80 (1958) 5090.

[4] R.M. Bowman, M. Dantus and A.H. Zewail, Chem. Phys. Letters 161 (1989) 297;
M. Dantus, R.M. Bowman and A.H. Zewail, Nature 343 (1990) 737.

[5] R.B. Bernstein and A.H. Zewail, Chem. Phys. Letters 170 (1990) 321;
M. Gruebele and A.H. Zewail, J. Chem. Phys. 98 (1993) 883.

[6] A.H. Zewail, M. Dantus, R.M. Bowman and A. Mokhtari, J. Photochem. Photobiol. A 62 (1992) 301.

[7] Y. Yang, R.M. Whitnell, K.R. Wilson and A.H. Zewail, Chem. Phys. Letters 193 (1992) 402.

[8] J. Troe, J. Phys. Chem. 90 (1986) 357;
J. Schroeder and J. Troe, Ann. Rev. Phys. Chem. 38 (1987) 163, and references therein.

[9] J.C. Dutoit, J.-M. Zellweger and H. van den Bergh, J. Chem. Phys. 78 (1983) 1825, and references therein.

[10] B. Otto, J. Schroeder and J. Troe, J. Chem. Phys. 81 (1984) 202.

[11] E.D. Potter, Q. Liu and A.H. Zewail, Chem. Phys. Letters 200 (1992) 605;
Q. Liu, J.-K. Wang and A.H. Zewail, Nature 364 (1993) 427.

[12] T.J. Chuang, G.W. Hoffman and K.B. Eisenthal, Chem. Phys. Letters 25 (1974) 201.

[13] D.J. Nesbitt and J.T. Hynes, J. Chem. Phys. 76 (1982) 6002; 77 (1982) 2130.

[14] P. Bado, C. Dupuy, D. Magde, K.R. Wilson and M.M. Malley, J. Chem. Phys. 80 (1984) 5531;
P. Bado and K.R. Wilson, J. Phys. Chem. 88 (1984) 655.

[15] N.A. Abul-Haj and D.F. Kelley, J. Phys. Chem. 91 (1987) 5903, and references therein.

[16] A.L. Harris, M. Berg and C.B. Harris, J. Chem. Phys. 84 (1986) 788;
M.E. Paige and C.B. Harris, Chem. Phys. 149 (1990) 37, and references therein.

[17] X. Xu, S. Yu, R. Lingle, H. Zhu and J.B. Hopkins, J. Chem. Phys. 95 (1991) 2445, and references therein.

[18] A.L. Harris, J.K. Brown and C.B. Harris, Ann. Rev. Phys. Chem. 39 (1988) 341.

[19] N.F. Scherer, L.D. Ziegler and G.R. Fleming, J. Chem. Phys. 96 (1992) 5544;
N.F. Scherer, D.M. Jonas and G.R. Fleming, J. Chem. Phys. 99 (1993) 153.

[20] R.J. Sension and H.L. Strauss, J. Chem. Phys. 85 (1986) 3791.

[21] J.Y. Bigot, M.T. Portella, R.W. Schoenlein, C.J. Bardeen, A. Migus and C.V. Shank, Phys. Rev. Letters 66 (1991) 1138.

[22] E.J. Nibbering, D.A. Wiersma and K. Duppen, Phys. Rev. Letters 66 (1991) 2464.

[23] B.A. Younglove, J. Phys. Chem. Ref. Data 11 Suppl. 1 (1982) 1-1;
R.B. Stewart, R.T. Jacobsen, J. Phys. Chem. Ref. Data 18 (1982) 639.
[24] J. Tellinghuisen, J. Chem. Phys. 58 (1973) 2821.
[25] J.C. Brand and A.R. Hoy, Can. J. Phys. 60 (1982) 1209.
[26] A.L. Guy, K.S. Viswanathan, A. Sur and J. Tellinghuisen, Chem. Phys. Letters 73 (1980) 582.
[27] J. Tellinghuisen, J. Mol. Spectry. 94 (1982) 231.
[28] M.J. Rosker, M. Dantus and A.H. Zewail, J. Chem. Phys. 89 (1988) 6113.
[29] S. Fei, X. Zheng, M.C. Heaven and J. Tellinghuisen, J. Chem. Phys. 97 (1992) 6057.
[30] K.S. Schweizer and D. Chandler, J. Chem. Phys. 76 (1982) 2296.
[31] M.R. Zakin and D.R. Herschbach, J. Chem. Phys. 89 (1988) 2380.
[32] D. Ben-Amotz, M.-R. Lee, S.Y. Cho and D.J. List, J. Chem. Phys. 96 (1992) 8781.
[33] J.I. Steinfeld, Accounts Chem. Res. 3 (1970) 313;
S. Churassy, F. Martin, R. Bacis, J. Vergès and R.W. Field, J. Chem. Phys. 75 (1981) 4863.
[34] T.L. Cottrell and J.C. McCoubrey, Molecular energy transfer in gases (Butterworths, London, 1961).
[35] G.A. Capelle and H.P. Broida, J. Chem. Phys. 58 (1973) 4212.
[36] K. Luther and J. Troe, Chem. Phys. Letters 24 (1974) 85.